

COMPARISON OF THE CRLC MODELS DESCRIBING THE HELMHOLTZ TYPE CELLS FOR THE NONDESTRUCTIVE PHOTOACOUSTIC SPECTROSCOPY

Lukasz Bartłomiej Chrobak, Mirosław Andrzej Maliński

*Technical University of Koszalin, Department of Electronics and Computer Science, Śniadeckich 2, 75-453 Koszalin, Poland
(✉ lukasz.chrobak@tu.koszalin.pl)*

Abstract

The photoacoustic cell is the heart of the nondestructive photoacoustic method. This article presents a new simple lumped-components CRLC model of the Helmholtz type photoacoustic cell. This model has been compared with the well known literature models describing the Helmholtz type cells for photoacoustic spectroscopy. Experimental amplitude and phase frequency data obtained for the two photoacoustic cells have been presented and interpreted in a series of models. Results of the fitting of theoretical curves, obtained in these models, to the experimental data have been shown and discussed.

Keywords: Nondestructive testing, photoacoustic spectroscopy, photoacoustic cells, Helmholtz cells

© 2014 Polish Academy of Sciences. All rights reserved

1. Introduction

Nowadays nondestructive photoacoustic spectroscopy has become an important tool for investigations of properties of materials widely used in the industry. Photoacoustic spectroscopy was successfully applied for gas detection [1], liquid measurements [2] or solid state investigations [3]. This method is based on acoustic wave generation resulting from the absorption of an intensity-modulated laser beam in the sample. The first theoretical background of the photoacoustic effect was presented by Rosencwaig and Gersho [4]. General requirements concerning the apparatus for measurements of the photoacoustic effect were presented in paper [5]. In the photoacoustic method a special cell with a microphone as the detector is used. The resonant Helmholtz cell [6] is one of the most often used cells in photoacoustics. The pressure response of the photoacoustic cell can be simulated by an electrical circuit with R, L and C electrical components. There are a few well known models describing this type of the photoacoustic cell [7–11]. However results of simulations obtained using these models are different i.e. they exhibit different frequency amplitude and phase characteristics. In the literature there also other alternative models are known. An improved transmission line model and a transmission line model after conversion of the line into a T-section are presented in paper [12]. A loss-improved electro-acoustical model has been described in paper [13]. In this work we present a comparison of the results obtained in different literature CRLC lumped components models, describing the Helmholtz type cells for photoacoustic spectroscopy. A new simple model is described and proposed in this paper.

2. Theory

In this section theoretical basics of several CRLC literature models have been presented and discussed. The new proposed model of a Helmholtz cell is also presented and discussed.

The Helmholtz resonator cell is an acoustic system of two volumes connected by a thin channel. A schematic diagram of an example of this cell type is presented in Fig.1.

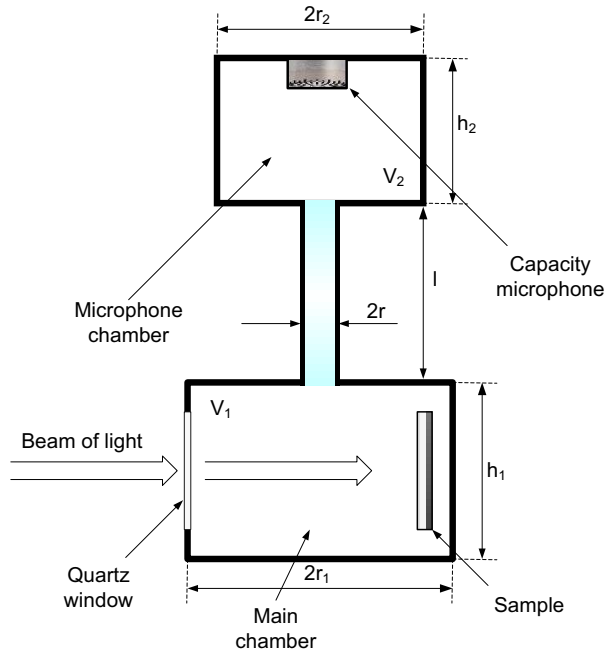


Fig. 1. A schematic diagram of the Helmholtz cell.

When the acoustic wavelength is much larger than the cell dimensions, the resonant system can be described by the electrical analog circuit presented in Fig.2.

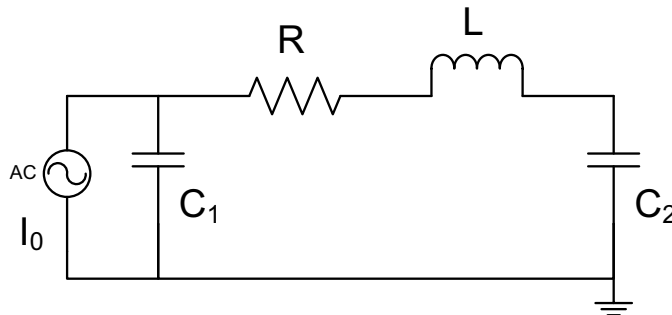


Fig. 2. An electric circuit analog of the photoacoustic Helmholtz cell.

Four different models describing electrical parts of the electric circuit presented in Fig.2 are presented in the literature. These models are presented below.

A model of Morse, Malecki:

$$C_i = \frac{V_i}{\rho v^2}, \quad R = \frac{\rho \eta l}{2\pi v}, \quad L = \frac{\rho l}{\pi r^2}. \quad (1)$$

A model of Blitz:

$$C_i = \frac{V_i}{\rho v^2}, \quad R = \frac{8\eta l}{\pi r^4}, \quad L = \frac{\rho l}{\pi r^2}. \quad (2)$$

A model of Nolle, Zyszkowski:

$$C_i = \frac{V_i}{\rho v^2}, \quad R = \frac{8\eta l}{\pi r^4}, \quad L = \frac{4}{3} \frac{\rho l}{\pi a^2}. \quad (3)$$

A model of Kastle, Sigrist:

$$C_i = \frac{V_i}{\rho v^2}, \quad R = \frac{l\sqrt{2\rho\omega}}{\pi r^3} \left[\sqrt{n} + \sqrt{\frac{k_g}{c_p}} (\kappa - 1) \right], \quad L = \frac{\rho l}{\pi r^2}. \quad (4)$$

A model of Mattiello:

$$C_i = \frac{V_i}{\rho v^2}, \quad R = l \sqrt{\frac{4\rho\pi f}{\pi r^3}}, \quad L = \frac{4\rho l}{\pi r^2}. \quad (5)$$

In this paper we propose a different model describing the electrical parts of the CRLC circuit.

$$C_i = \frac{M V_i}{N_a k T \rho} = \frac{\kappa V_i}{\rho v^2}, \quad R = \frac{8\eta l}{\pi r^4}, \quad L = \frac{\rho l}{\pi r^2}. \quad (6)$$

Where: l is the resonant channel length, r is the channel radius, ρ is air density, M is the mole mass of the gas, V_i is the volume of the photoacoustic cell ($i=1$) and microphone chamber ($i=2$), N_a is the Avogadro number, k is the Boltzman constant, T is the gas temperature, $\kappa=c_p/c_v$, ω is circular modulation frequency of the intensity of the laser beam and η is air viscosity.

To compare the proposed model with the other models it was necessary to normalize variables describing the individual components. In this situation we wrote the velocity of sound in a different form, expressed by the physical parameters of air (7–10).

$$v = \sqrt{\frac{Y}{\rho}}, \quad (7)$$

$$\frac{\Delta V}{V} = \frac{1}{Y} \Delta P, \quad (8)$$

$$Y = \kappa P_0 \quad Y = \kappa \frac{\rho k T N_A}{M}, \quad (9)$$

$$v = \sqrt{\frac{\kappa N_A k T}{M}}. \quad (10)$$

All values of physical constants and parameters of air used for computations in this paper have been presented in Tab.1.

Table 1. Physical constants and air parameters used in this paper.

Constant name	Constant dimension
Air density	$\rho = 1.168 \text{ kg / m}^3$
Air viscosity	$\eta = 1.7 \cdot 10^{-5} \text{ kg / ms}$
Mole mass of air	$M = 0.028 \text{ kg/mol}$
Avogadro constant	$N_A = 6.022 \cdot 10^{23} \text{ mol}^{-1}$
Boltzman constant	$k = 1.38 \cdot 10^{-23} \text{ J / K}$

The amplitude and phase frequency characteristics of the photoacoustic (PA) signal with the use of the Helmholtz type cell, in the CRLC model, can be expressed as:

$$Amp(\omega) = \left| \frac{I}{\omega[-jC_1C_2L\omega^2 - C_1C_2R\omega + j(C_1 + C_2)]} \right|, \quad (11)$$

$$Ph(\omega) = \frac{180}{\pi} \arg \left(\frac{I}{\omega[-jC_1C_2L\omega^2 - C_1C_2R\omega + j(C_1 + C_2)]} \right). \quad (12)$$

The collection of formulae describing the resonant frequency in different models is presented in Table 2.

Table 2. Formulae for the resonant frequency in different models.

Authors of the model	Resonant Frequency Formulae	Modified Resonant Frequency Formulae
Morse, Malecki	$\frac{1}{2\sqrt{\pi} \sqrt{\frac{LV_1V_2}{r^2v^2(V_1+V_2)}}}$	$\frac{\sqrt{2}}{4\sqrt{\pi} \sqrt{\frac{LMV_1V_2}{3N_aTkr^2(V_1+V_2)}}}$
Blitz	$\frac{1}{2\sqrt{\pi} \sqrt{\frac{LV_1V_2}{r^2v^2(V_1+V_2)}}}$	$\frac{\sqrt{2}}{4\sqrt{\pi} \sqrt{\frac{LMV_1V_2}{3N_aTkr^2(V_1+V_2)}}}$
Nolle, Żyszkowski	$\frac{1}{4\sqrt{\pi} \sqrt{\frac{LV_1V_2}{3r^2v^2(V_1+V_2)}}}$	$\frac{\sqrt{2}}{8\sqrt{\pi} \sqrt{\frac{LMV_1V_2}{9N_aTkr^2(V_1+V_2)}}}$
Kastle, Sigrist	$\frac{1}{2\sqrt{\pi} \sqrt{\frac{LV_1V_2}{r^2v^2(V_1+V_2)}}}$	$\frac{\sqrt{2}}{4\sqrt{\pi} \sqrt{\frac{LMV_1V_2}{3N_aTkr^2(V_1+V_2)}}}$
Mattiello	$\frac{1}{4\sqrt{\pi} \sqrt{\frac{LV_1V_2}{r^2v^2(V_1+V_2)}}}$	$\frac{\sqrt{2}}{8\sqrt{\pi} \sqrt{\frac{LMV_1V_2}{3N_aTkr^2(V_1+V_2)}}}$
Proposed model	$\frac{\sqrt{3}}{6\sqrt{\pi} \sqrt{\frac{3LV_1V_2}{2r^2v^2(V_1+V_2)}}}$	$\frac{1}{2\sqrt{\pi} \sqrt{\frac{LMV_1V_2}{N_aTkr^2(V_1+V_2)}}}$

Limitations of the presented model are based on the cell dimensions (the acoustic wavelength is much larger than the resonator dimensions and the channel volume is considerably smaller compared to the volumes of the microphone chamber and the main chamber). For example, the proposed model would not be suitable for the open Helmholtz cell or the open windowless Helmholtz cell proposed by Starecki [14]. In this case the transmission line model with loss corrections of Starecki could be used [13].

3. Experimental results

For the comparison of the discussed models we used two different photoacoustic cells and performed frequency PA amplitude and phase measurements for the thermally thick black carbon sample.

Dimensions of the first Helmholtz cell were the following: $r_1=3$ mm, $h_1=3$ mm for the main chamber, $r=0.6$ mm and $d=15$ mm for the channel, and $r_2=6.3$ mm, $h_2=1.5$ mm for the microphone chamber. This cell is described elsewhere [15]. This cell was used successfully for wide spectra of different photoacoustic investigations [16–18].

The experimental and theoretical amplitude and phase PA frequency characteristics obtained for this cell are presented in Figs.3 and 4.

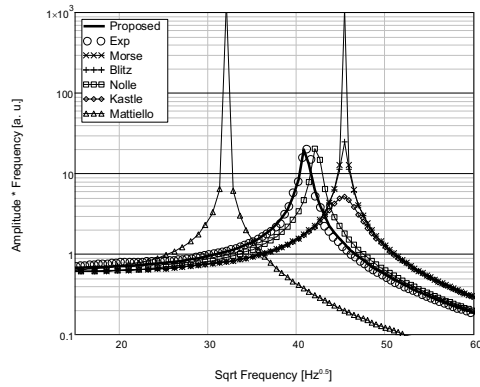


Fig. 3. Amplitude of the photoacoustic signal times the frequency of modulation versus the square root of the frequency of modulation obtained for the thermally thick black carbon sample. The thick solid line is a theoretical curve computed for the proposed model, the remaining lines are theoretical curves computed for different models known from the literature, circles are experimental points.

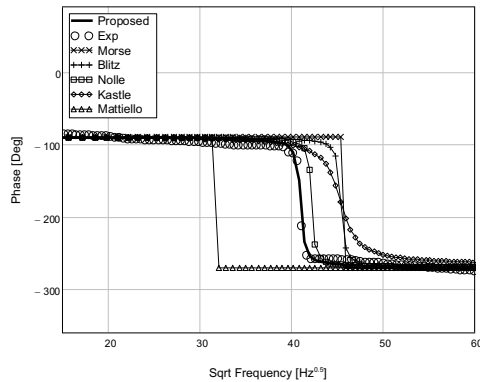


Fig. 4. Phase of the photoacoustic signal versus the square root of the frequency of modulation obtained for the thermally thick black carbon sample. The thick solid line is a theoretical curve computed for the proposed model, the remaining lines are theoretical curves computed for different models known from literature, circles are experimental points.

Table 3. The comparison of resonant frequency values calculated for different models with the experimental value.

Authors of the model	Resonant Frequency [Hz]
Morse, Malecki	2059
Blitz	2059
Nolle, Żyszkowski	1783
Kastle, Sigrist	2059
Mattiello	1030
Proposed model	1676
Experimental value	1689

For a better comparison the second PA cell has been used. Dimensions of the second PA cell were the following: $r_1=4$ mm, $h_1=2$ mm for the main chamber $r=0.2$ mm and $d=3$ mm for the channel and $r_2=2$ mm, $h_2=2$ mm for the microphone chamber. In this cell a standard electret microphone has been used.

The experimental and theoretical amplitude and phase PA frequency characteristics obtained for this cell are presented in Figs.5 and 6.

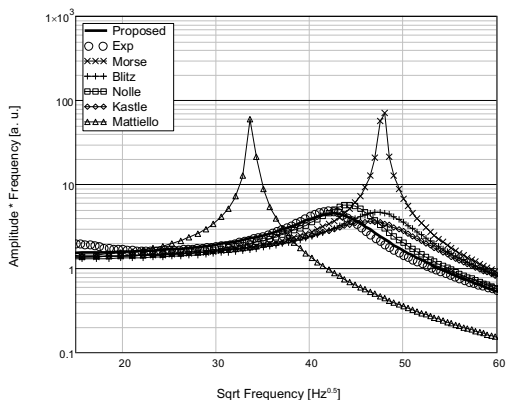


Fig. 5. Amplitude of the photoacoustic signal times the frequency of modulation versus the square root of the frequency of modulation obtained for the thermally thick black carbon sample. The thick solid line is a theoretical curve computed for the proposed model, the remaining lines are theoretical curves computed for different models known from literature, circles are experimental points.

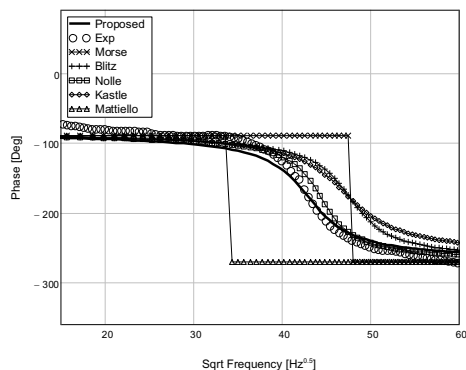


Fig. 6. Phase of the photoacoustic signal versus the square root of the frequency of modulation obtained for the thermally thick black carbon sample. The thick solid line is a theoretical curve computed for the proposed model, remaining lines are theoretical curves computed for different models known from literature, circles are experimental points.

The experimental and theoretical values of resonant frequencies computed for the second PA cell, for different models, are presented in Table 4.

Table 4. The comparison of resonant frequency values calculated for different models with the experimental value.

Authors of the model	Resonant Frequency [Hz]
Morse, Malecki	2284
Blitz	2284
Nolle, Żyszkowski	1951
Kastle, Sigrist	2284
Mattiello	1142
Proposed model	1773
Experimental value	1764

4. Conclusions

In this work we propose a new, simple lumped-components CRLC model describing the Helmholtz photoacoustic cell. The comparison of amplitude and phase PA theoretical characteristics, computed for a series of literature models of the PA resonant Helmholtz cell, with the experimental PA characteristics obtained for two, designed and performed, Helmholtz cells whose dimensions were well known, proved that the proposed model enables the best fitting of both theoretical curves to experimental frequency characteristics and the experimental resonant frequency of the cell.

References

- [1] Rey, J. M., Romer, C., Gianella, M., Sigrist, M. W. (2010). Near-infrared resonant photoacoustic gas measurement using simultaneous dual-frequency excitation. *Appl. Phys. B* 100(1), 189–194.
- [2] Chrobak, Ł., Maliński, M., Patryn, A. (2011). Influence of Plasma Waves on the Photoacoustic Signal of Silicon Samples. *International Journal of Thermophysics* 32(9), 1986–1997.
- [3] Balderas-Lopez, J. A., Gutierrez-Juarez, G., Jaime-Fonseca, M. R., Sanchez-Sinencio, F. (1999). Measurements of thermal effusivity of liquids using a conventional photoacoustic cell. *Rev. Sci. Instrum.* 70(4), 2069–2071.
- [4] Rosencwaig, A., Gersho, A. (1976). Theory of the photoacoustic effect with solids. *J. Appl. Phys.* 47(1), 64–74.
- [5] Rosencwaig, A. (1997). Photoacoustic spectroscopy of solids. *Rev. Sci. Instrum.*, 48(9), 1133–1138.
- [6] Fernelius, N. C. (1979). Helmholtz resonance effect in photoacoustic cells. *Appl. Opt.* 18(11), 1784–1787.
- [7] Morse, P. M. (1948). *Vibration and sound*. McGraw-Hill, New York.
- [8] Blitz, J. (1964). *Elements of acoustics*. Butterworths, London.
- [9] Nolle, A. W. (1953). Small – signal impedance of short tubes. *J. Acoust. Soc. Am.* 25(1), 32–39.
- [10] Kastle, R., Sigrist, M. W. (1996). Temperature dependent photacoustics spectroscopy with a Helmholtz resonator. *Appl. Phys. B* 63(4), 389–397.
- [11] Mattiello, M. (2006). Novel Helmholtz-based photoacoustic sensor for trace gas detection at ppm level using GaInAsSb/GaAlAsS DFB lasers. *Spectrochim. Acta A* 63(5), 952–958.
- [12] Starecki, T. (2005). Practical improvements of modeling of photoacoustic Helmholtz cells. *Proc. SPIE* 6159, 653–658.
- [13] Starecki, T. (2007). Loss – improved electro acoustical modeling of small Helmholtz resonators. *J. Acoust. Soc. Am.* 122, 2118–2123.
- [14] Starecki, T. (2008). Windowless Open Photoacoustic Helmholtz Cell. *Acta Physica Polonica A*, 114, 211–216.
- [15] Chrobak, Ł., Maliński, M. (2013). Design and optimization of the photoacoustic cell for nondestructive photoacoustic spectroscopy. *Nondestructive Testing and Evaluation* 28(1), 17–27.
- [16] Maliński, M., Chrobak, Ł., Zakrzewski, J., Strzałkowski, K. (2011). Photoacoustic Method of Determination of Quantum Efficiency of Luminescence in Mn^{2+} Ions in $Zn_{1-x-y}Be_xMn_ySe$ Crystals. *Opto-Electronics Review* 19(2), 183–188.
- [17] Chrobak, Ł., Maliński, M., Zakrzewski, J., Strzałkowski, K. (2010). The Photoacoustic Spectroscopic Investigations of the Surface Preparation of ZnSe Crystals with the use of the Optimization Methods. *Applied Surface Science* 256, 2458–2461.
- [18] Maliński, M., Chrobak, Ł., Patryn, A. (2009). Theoretical and Experimental Studies of a Plasma Wave Contribution. *Acta Acustica united with Acustica* 95, 60–64.